

# **Anomalous size effects of effective stiffnesses in bistable counter-rotating mechanical metamaterials**

Zehuan Tang, Tingfeng MA<sup>\*</sup>, Boyue Su, Pengfei Kang, Bowei Wu, Hui Chen<sup>\*</sup>,  
Shuanghuizhi Li, Decai Wu, Yujie Zhang, Gen Zhao

School of Mechanical Engineering and Mechanics, Ningbo University, Ningbo  
315211, China

## **ABSTRACT**

Counter-rotating mechanical metamaterials have previously been found to have anomalous characteristics or functions such as auxetics effects, shape changers, and soliton transports, which are all under monostable conditions. The properties of counter-rotating mechanical metamaterials under bistable conditions have not yet been explored. Here, we found that for a bistable counter-rotating metamaterial chain, the effective stiffnesses of the two steady states are different in the chain with even-numbered nodes. For the chain with odd-numbered nodes, the effective stiffnesses corresponding to the two steady states are exactly the same. This special property is not characterized by the characteristic attenuation lengths of the underlying mechanism, but depends on the different symmetries of the underlying mechanism of the chains with odd and even nodes. In addition, the relationship between the abnormal non-monotonic size effect and equilibrium angle are clarified. More interestingly, for one-dimensional chains with even-numbered nodes, the size effect of effective stiffness bifurcates at a specific equilibrium angle, and the according mechanisms are revealed.

Key words: Anomalous size effect; Effective stiffness; Bistable counter-rotating metamaterials; Bifurcating

## **1.Introduction**

In recent years, mechanical metamaterials have attracted a lot of attentions due to unusual mechanical properties, such as negative stiffness [1-2], negative Poisson ratio [3] and adjustable Poisson ratio [4], et al., and thus provided a new platform for the control of static and dynamic mechanical properties.

Most mechanical metamaterials exhibit size effects under loadings due to the influences of their internal geometry on the overall deformation [5-7]. This size effect could be positive or negative. A kind of positive size effect has been predicted in the generalized continuum theory, such as micropolar, couple stress, and gradient elasticity [8, 9]. In addition, positive size effects have been observed in various heterogeneous materials [10-13]. On the other hand, in hard biological tissues, negative size effects have been observed [7,14], namely the compliance increases with the size reduction [15]. The size effects in the above studies are typically monotonous. However, in many complicated application scenarios, such as deformation control of lightweight robots, and intelligent structural unit in aerospace, non-monotonic size effects is vital to obtain self-adaptation controls. Thus it is necessary to investigate non-monotonic rules of size effects in mechanical metamaterials.

It has been proved that by using counter-rotating mechanical metamaterials, the auxetics effect [16], topological insulators [17], and soliton transports [18, 19] could be realized. The responses of this kind of metamaterials are closely related to the underlying mechanism. For example, for soliton collisions, positive and negative soliton amplitudes can modify the underlying mechanism to achieve anomalous soliton collisions [20]. Some interesting size effects emerges in monostable counter-rotating metamaterials [21]: the effective stiffness of the chains with odd and

even-numbered nodes differs greatly at small sizes, but almost coincides at large sizes. This is because the attenuation lengths of finite chains with odd and even-numbered nodes converge to the characteristic attenuation lengths of periodic structures when the size (number of nodes) is large enough. In particular, a non-monotonic size effect is observed for the effective stiffness of a monostable chain with even-numbered units.

The multistable design can significantly expand the functional range of counter-rotating metamaterials. For example, for the solitary wave propagations, the bistable chain can be used as a carrier of topological soliton propagations [22], and the transition wave can form a static domain wall when the tristable chain collides [23]. However, the design of multistable state makes the underlying mechanism of counter-rotating metamaterial more complicated, thus the size effect of multistable counter-rotating metamaterial chain has not been revealed, which affects the design of intelligent mechanism. Abnormal size effects of multistable counter-rotating metamaterial chains need to be explored.

In this paper, the abnormal size effects of the effective stiffness of bistable counter-rotating metamaterial chains are explored by theoretical and experimental methods, and the formation mechanisms are revealed, which can provide an important basis for designs of complicated intelligent mechanisms in robots in the future.

## **2. Bistable counter-rotating mechanical metamaterial chains**

A bistable mechanical metamaterial chain consisting of  $M+1$  nodes is considered, as shown in Fig. 1(a). Each node is composed of two crosses, and each cross consists of a T-shaped frame and two L-shaped frames. A linear spring is attached to mass centers of the upper and lower crosses. Besides, two adjacent crosses

are connected by a thin elastic shim. The parameters of the cross include mass  $m$ , moment of inertia  $J$ , arm length  $l$  and slim length  $l_h$ . As shown in Fig. 1(b), the elastic slim is modeled as a combination of stretch, shear, and torsional springs, the parameters of which include flexural stiffness  $k_\theta$ , shear stiffness  $k_s$ , and tension stiffness  $k_l$ , and the transverse displacement and rotation-angle at the  $n$ th cross are denoted by  $u_n$  and  $\delta\theta_n$ , respectively, and two adjacent units rotate in opposite directions.

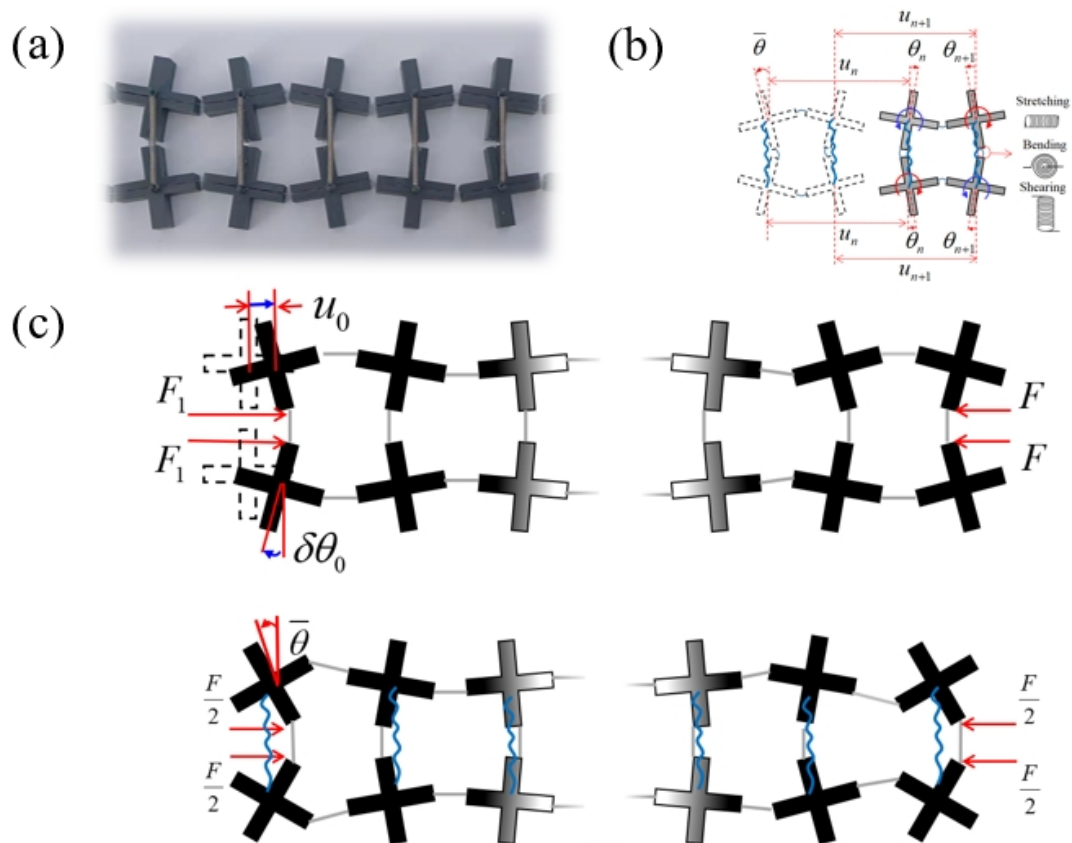


Fig. 1. (a) Photos of local nodes of the bistable chain. (b) Schematic diagram of the model. (c) Schematic diagram of the finite chain model (the shown chain is composed of even-numbered nodes)

### 3. Mathematical model

#### 3.1 Discrete model

A force  $F$  is applied to the connection points between the slims and the crosses at

two ends, as shown in Fig. 1(c), the governing equations for displacements are established as follows:

$$0 = k_l[(u_1 - u_0) + l \sin \bar{\theta}(\delta\theta_1 + \delta\theta_0)] + F/2, \quad (1-a)$$

$$0 = k_l[u_{n+1} + u_{n-1} - 2u_n + l \sin \bar{\theta}(\delta\theta_{n+1} - \delta\theta_{n-1})], n \in [1, M-1] \quad (1-b)$$

$$0 = k_l[(u_{M-1} - u_M) - l \sin \bar{\theta}(\delta\theta_{M-1} + \delta\theta_M)] - F/2. \quad (1-c)$$

The governing equations for rotation-angles are established as follows:

$$0 = -k_\theta(\delta\theta_1 + 3\delta\theta_0) - k_l(\delta\theta_1 + \delta\theta_0)l^2 \sin^2 \bar{\theta} + k_s(\delta\theta_1 - \delta\theta_0)l^2 \cos \bar{\theta} - k_t 2\delta\theta_0 \sin \bar{\theta}^2 \sin \bar{\theta} + Fl \cos \bar{\theta} / 2 - k_l[(u_1 - u_0)l \sin \bar{\theta}], \quad (2-a)$$

$$0 = -k_\theta(\delta\theta_{n+1} + \delta\theta_{n-1} + 4\delta\theta_n + 6\bar{\theta}) - k_l((u_{n+1} - u_{n-1}) + l \sin \bar{\theta}(2\delta\theta_n + \delta\theta_{n+1} + \delta\theta_{n-1}))l \sin \bar{\theta}, n \in [1, M-1] - k_s(\delta\theta_{n+1} + \delta\theta_{n-1} - 2\delta\theta_n)l^2 \cos \bar{\theta} + k_t(2\cos \bar{\theta} - 2\delta\theta_n \sin \bar{\theta} - \beta)l^2 \sin \bar{\theta} \quad (2-b)$$

$$0 = -k_\theta(\delta\theta_{M-1} + 3\delta\theta_M) - k_l(\delta\theta_M + \delta\theta_{M-1})l^2 \sin^2 \bar{\theta} + k_s(\delta\theta_{M-1} - \delta\theta_M)l^2 \cos \bar{\theta} - k_t 2\delta\theta_M \sin \bar{\theta}^2 \sin \bar{\theta} \pm Fl \cos \bar{\theta} / 2 - k_l(u_M - u_{M-1})l \sin \bar{\theta}, \quad (2-c)$$

where  $\beta$  is a characteristic quantity defined as  $\beta = (l_0 - l_h)/l$ . In Eq.(2-c), for the item  $\pm Fl \cos \bar{\theta}$ , the positive sign is selected for the chain with even-numbered nodes, and the negative sign is selected for that with odd-numbered nodes. According to Eqs.(1) and (2), the displacement and rotation angle are completely decoupled when  $\bar{\theta} = 0$  (monostable chain), while those are coupled when  $\bar{\theta} \neq 0$  (bistable chain), and the coupling extent increases with the increase of  $\bar{\theta}$ . Eqs.(1) and (2) are rewritten in the matrix form:

$$[\mathbf{F}] = [\mathbf{K}][\tilde{\mathbf{U}}], \quad (3)$$

where,  $[\mathbf{F}] = [F/2, Fl \cos \bar{\theta} / 2, 0, \dots, 0, -F/2, -Fl \cos \bar{\theta} / 2]^T$  is the matrix composed of external forces,  $[\mathbf{K}]$  is the total rigid matrix of the finite chain of  $M+1$  nodes,

and  $\tilde{\mathbf{U}} = [u_0, \delta\theta_0, u_1, \dots, \delta\theta_{N-1}, u_N, \delta\theta_N]^T$  is the matrix of the rotation angle and displacement of each node. The effective stiffness of the one-dimensional chain can be written as:

$$k_e = \frac{F}{\Delta L_e} = \frac{F}{u_0 - u_M + l(\delta\theta_0 \pm \delta\theta_M)}. \quad (4)$$

In Eq. (4), for the item  $\pm\delta\theta_M$ , the positive sign is selected for the chain with even-numbered nodes, and the negative sign is selected for that with odd-numbered nodes. Numerical solutions of  $\tilde{\mathbf{U}}$  can be obtained from Eq. (3), then substitute that into the definition expression of effective stiffness (Eq.(4)), thus the effective stiffness from the discrete model can be obtained.

### 3.2 Continuous Model

In order to better capture abnormal size effects, a continuous model of bistable chain is established. For the governing equations Eqs. (1-b) and (2-b) for  $n \in [1, M-1]$ , the form in the continuum limit is considered. Several variables are normalized as follows:  $K_s = k_s / k_t$ ,  $K_t = k_t / k_t$ ,  $X = x / (2l \cos \bar{\theta})$ . Assuming that the envelopes of the rotation-angle and displacement fields have a small gradient, the continuous rotation-angle field  $\delta\theta(X)$  and displacement field  $u(X)$  are introduced, satisfying  $\delta\theta_n = \delta\theta(X_n)$  and  $u_n = u(X_n)$ . By expanding  $\delta\theta_{n\pm 1} = \delta\theta(X_n \pm 1)$  and  $u_{n\pm 1} = u(X_n \pm 1)$  in Taylor's series, we obtain:

$$\delta\theta_{n\pm 1} = \delta\theta(X_n) \pm \partial_X \delta\theta(X_n) + \partial_{XX} \delta\theta(X_n) / 2, \quad (5-a)$$

$$u_{n\pm 1} = u(X_n) \pm \partial_X u(X_n) + \partial_{XX} u(X_n) / 2. \quad (5-b)$$

By substituting Eqs. (5-a) and (5-b) into Eqs. (1-b) and (2-b), we obtain:

$$\tan \bar{\theta} \frac{\partial \delta\theta}{\partial X} + \frac{\partial^2 U}{\partial X^2} = 0, \quad (6)$$

$$\begin{aligned}
& -K_\theta \left( \frac{\partial^2 \delta\theta}{\partial X^2} + 6\delta\theta \right) - \left( 4 \frac{\partial U}{\partial X} \cos \bar{\theta} + 4 \sin \bar{\theta} \delta\theta \right) \sin \bar{\theta} \\
& + K_s \left( \frac{\partial^2 \delta\theta}{\partial X^2} \right) \cos \bar{\theta} - 2K_t \delta\theta \sin^2 \bar{\theta} = 0,
\end{aligned} \tag{7}$$

where  $U = u / (2l \cos \bar{\theta})$ . For periodic boundaries, since the boundary condition at infinity can be seen as an asymptotic state (the gradient of the field at infinity goes to zero), Eq.(7) can be simplified by integrating Eq.(6). However, when the force  $F$  is applied to both ends of the chain, the changes in displacement and rotation-angle of the chain from boundary states at its two ends, and the changes at both ends are the largest in the whole chain, namely, the condition that infinity is an asymptotic state is not satisfied. Thus by taking the derivation of Eq.(7), we obtain:

$$\begin{aligned}
& -K_\theta \left( \frac{\partial^3 \delta\theta}{\partial X^3} + 6 \frac{\partial \delta\theta}{\partial X} \right) - \left( 4 \frac{\partial^2 U}{\partial X^2} \cos \bar{\theta} + 4 \sin \bar{\theta} \frac{\delta\theta}{\partial X} \right) \sin \bar{\theta} \\
& + K_s \left( \frac{\partial^3 \delta\theta}{\partial X^3} \right) \cos \bar{\theta} - 2K_t \frac{\delta\theta}{\partial X} \sin^2 \bar{\theta} = 0.
\end{aligned} \tag{8}$$

Eq.(7) is the definite conditions for solving partial differential equations Eq. (8), and substituting Eq. (6) into Eq. (8) yields:

$$\frac{\partial^3 \delta\theta}{\partial X^3} - \frac{1}{(\lambda^*)^2} \frac{\delta\theta}{\partial X} = 0, \tag{9}$$

where  $\lambda^* = \sqrt{(K_s \cos \bar{\theta} - K_\theta) / (6K_\theta + 2K_t \sin^2 \bar{\theta})}$ .

### 3.2.1 Continuous model for the chain with even-numbered nodes

Eq.(9) is a third-order linear equation of rotation-angle  $\theta$ , and its solution is composed of the linear combination of  $e^{X/\lambda^*}$  and  $e^{-X/\lambda^*}$ . For chains with even-numbered nodes, the symmetric structure is under the symmetric force system, thus the displacement and rotation-angle at the left and right ends satisfy the variable substitution, namely  $u_n^+ = -u_{M-n}^+$  and  $\delta\theta_n^+ = \delta\theta_{M-n}^+$ . The rotation-angle solution can be written as:

$$\delta\theta = C_1(e^{X/\lambda^*} + e^{(M-X)/\lambda^*}) + C_0, \quad (10)$$

where  $\lambda^*$  is the characteristic attenuation length of the bistable chain,  $C_1$  and  $C_0$  are the integral constants. Substituting Eq. (10) into Eq. (6) yields:

$$U = -\tan\bar{\theta}\lambda^*C_1(e^{X/\lambda^*} - e^{(M-X)/\lambda^*}) + \frac{D_1(2X-M)}{2l\cos\bar{\theta}}, \quad (11)$$

where  $D_1$  is the integral constant. By substituting Eqs. (10) and (11) into Eq. (7), a governing equation of three integral constants is obtained:

$$(3K_0 + 2\sin^2\bar{\theta} + K_l\sin^2\bar{\theta})C_0 + \frac{2\sin\bar{\theta}}{l}D_1 = 0. \quad (12)$$

Combined with the boundary conditions, Eq. (12) can be used to determine the values of the three integral constants. The governing equations Eqs.(1-a), (1-c), (2-a), and (2-c) for the left and right ends can be considered as the boundary conditions. The structure satisfies the axial symmetry, thus boundary conditions Eqs.(1-a) and (2-c) at the left end are enough. By combining obtained two governing equations and Eq.(12), the governing equations of three integral constants are obtained:

$$[F] = [\bar{K}]_{\text{even}} [C], \quad (13)$$

where  $[C] = [C_1, C_0, D_1]^T$  is the matrix composed of integral constants,  $[F]$  is the non-homogeneous term about the external force  $F$ ,  $[\bar{K}]_{\text{even}}$  is a  $3 \times 3$  coefficient matrix. By substituting the integral constants obtained by Eq. (13) into expressions of the displacement and rotation-angle solutions (Eqs.(10) and (11)), and substituting the obtained solutions into the definition expression of the effective stiffness  $k_e = F/[u_0 - u_N + l(\delta\theta_0 + \delta\theta_M)]$ , the effective stiffness of the chain with even-numbered nodes from the continuous model can be obtained. It can be seen from Eq.(13) that all three integral constants are proportional to the external force  $F$ ,



namely, the displacement and rotation-angle solutions are proportional to the external force  $F$ , which indicates that the effective stiffness remains unchanged with the change of  $F$ . This is a significant feature of a linear system.

### 3.2.2 Continuous model for the chain with odd-numbered nodes

For chains with odd-numbered nodes, although the force system acts symmetrically, the structure is not axisymmetric under this force system, as shown in Fig. 2. Therefore, axisymmetry cannot be used to simplify the model, and the solution form is as follows:

$$\delta\theta_n = (C_1 e^{n/\lambda^*} - C_2 e^{-n/\lambda^*}) / \lambda^* + C_0. \quad (14)$$

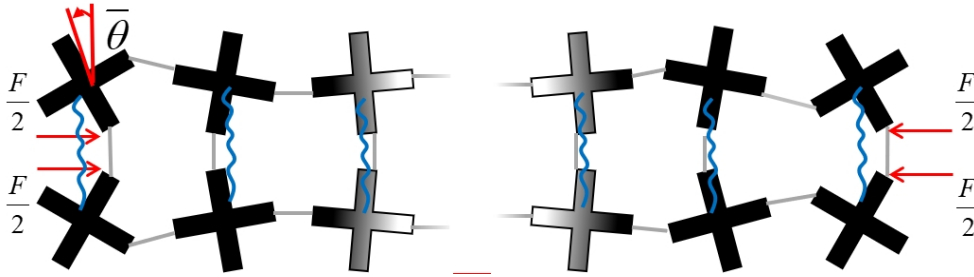


Fig. 2. Schematic diagram of the finite chain composed of odd-numbered nodes

The Eq. (13) is substituted into the displacement governing equation Eq. (6), a second-order linear equation is obtained and further solved, and the displacement solution is obtained:

$$U = -\tan \bar{\theta} (n^*)^2 (C_1 e^{n/n^*} + C_2 e^{-n/n^*}) + \frac{D_1 X + D_2}{2l \cos \theta}, \quad (15)$$

where  $C_1, C_2, C_0, D_1, D_2$  are five integral constants. By substituting Eqs. (14) and (15) into Eqs. (1-a), (1-c), (2-a) and (2-c), four governing equations are obtained and further combined with Eq. (12), then the governing equations of five integration constants are obtained:

$$[F] = [\bar{K}]_{\text{odd}} [C], \quad (16)$$

where  $[C]=[C_1, C_2, C_\theta, D_1, D_2]^T$  is the matrix composed of the integral constants,  $[F]$  is the non-homogeneous term about the external force  $F$ ,  $[\bar{K}]_{\text{odd}}$  is a  $5 \times 5$  coefficient matrix. The effective stiffness of the chain with odd-numbered nodes can be obtained by substituting the rotation-angle and displacement solutions into the definition of the effective stiffness  $k_e = F/[u_0 - u_N + l(\delta\theta_0 - \delta\theta_N)]$ . Four boundary conditions of the chain with odd-numbered nodes for the initial equilibrium angle  $\bar{\theta}$  are as follows:

$$0 = k_l[(u_1 - u_0) + l \sin \bar{\theta}(\delta\theta_1 + \delta\theta_0)] + F/2,$$

$$0 = k_l[(u_{N-1} - u_N) - l \sin \bar{\theta}(\delta\theta_{N-1} + \delta\theta_N)] - F/2,$$

$$0 = -k_\theta(\delta\theta_1 + 3\delta\theta_0) - k_l(\delta\theta_1 + \delta\theta_0)l^2 \sin^2 \bar{\theta} + k_s(\delta\theta_1 - \delta\theta_0)l^2 \cos \bar{\theta} \\ - k_l 2\delta\theta_0 \sin \bar{\theta}^2 \sin \bar{\theta} + Fl \cos \bar{\theta} / 2 - k_l[(u_1 - u_0)l \sin \bar{\theta},$$

$$0 = -k_\theta(\delta\theta_{N-1} + 3\delta\theta_N) - k_l(\delta\theta_N + \delta\theta_{N-1})l^2 \sin^2 \bar{\theta} + k_s(\delta\theta_{N-1} - \delta\theta_N)l^2 \cos \bar{\theta} \\ - k_l 2\delta\theta_N \sin \bar{\theta}^2 \sin \bar{\theta} - Fl \cos \bar{\theta} / 2 - k_l(u_N - u_{N-1})l \sin \bar{\theta}.$$

For the above boundary conditions, by replacing  $\bar{\theta}$  with  $-\bar{\theta}$ , those for the initial equilibrium angle  $-\bar{\theta}$  are obtained. The displacement distribution  $u_n^-$  and rotation-angle distribution  $\delta\theta_n^-$  for initial equilibrium angle  $-\bar{\theta}$  can be obtained by variable substitutions, namely,

$$u_n^- = -u_{M-n}^+; \delta\theta_n^- = -\delta\theta_{M-n}^+. \quad (17)$$

From Eq.(17), it is indicated that one-dimensional chains with odd-numbered nodes are mirrorsymmetric before and after the equilibrium angle inversion, as shown in Fig.

3.

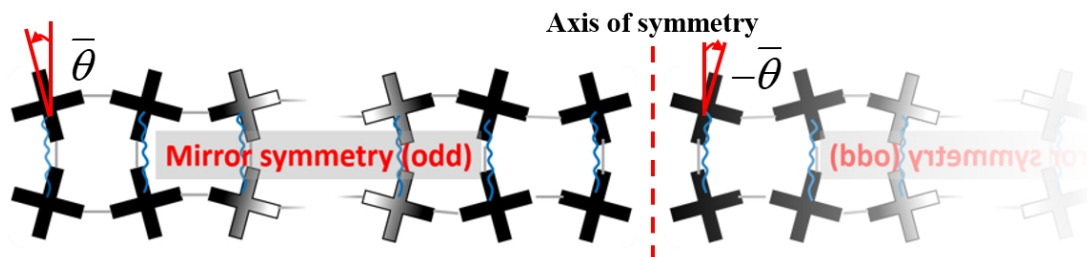


Fig. 3. Schematic diagram of the mirror symmetry in the finite chain composed of odd-numbered nodes

### 3 Abnormal size effects of effective stiffnesses

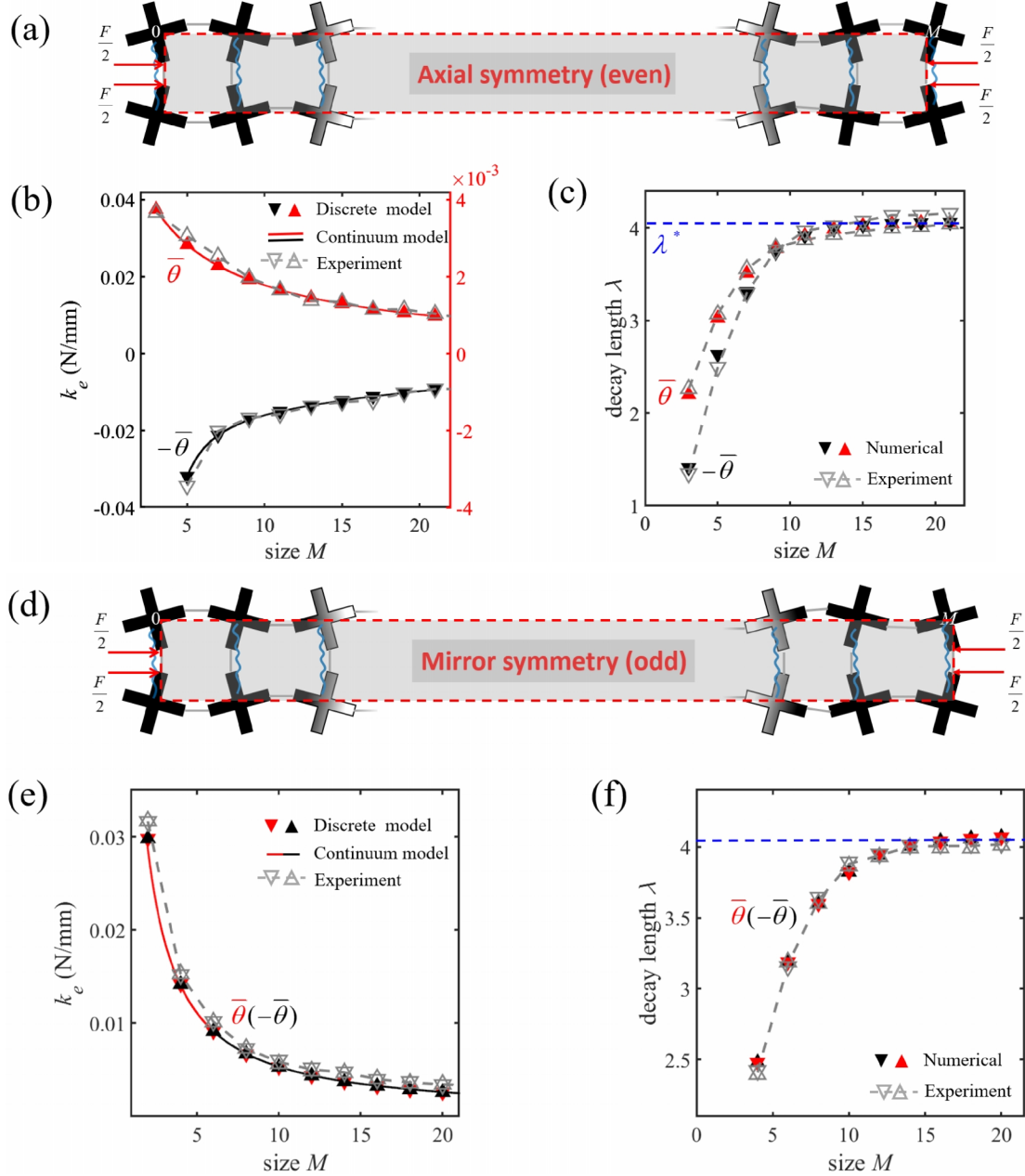


Fig. 4. (a) The force diagram of the chain with even-numbered nodes, the chain is symmetric about the middle axis. (b) The stiffness vs. node number  $M$  of the chain with even-numbered nodes. (c) When the chain has even-numbered nodes, the attenuation length of the chains with initial equilibrium angles  $\pm\bar{\theta}$  converges to the characteristic attenuation length  $\lambda^*$ . (d) The force diagram of the chain with odd-numbered nodes, and the chain with an initial equilibrium angle  $\bar{\theta}$  can be transformed into that with an initial equilibrium angle  $-\bar{\theta}$  through mirror symmetry. (e) The change stiffness vs.  $M$  of the chain with odd-numbered

nodes. (f) When the chain has odd-numbered nodes, the attenuation length of the chain with initial equilibrium angles  $\pm\bar{\theta}$  converges to the characteristic attenuation length  $\lambda^*$ .

The effective stiffnesses of the one-dimensional counter-rotating metamaterial chain in Fig. 4 (a) are solved theoretically and numerically, and corresponding experimental tests are also carried out. The parameters are set as follows:  $l_h = 0.02$  mm,  $k_l = 40$  N/mm,  $k_s = 0.191$  N/mm,  $k_\theta = 0.0608$  N/mm.

A force is applied on the connection points of the slims and the crosses at both ends, the force diagrams of the chain with even- and odd-numbered nodes are shown in Figs. 4(a) and 4(d), respectively. The effective stiffnesses of the chain with even-numbered nodes are shown in Fig. 4(b) (triangles in the figure represent the results from discrete models, and solid lines represent the results from continuous models), where the red triangles correspond to the results for  $\bar{\theta}$ , and the black triangles correspond to the results for  $-\bar{\theta}$ . Fig. 4(b) shows that the effective stiffnesses under initial equilibrium angles  $\bar{\theta}$  and  $-\bar{\theta}$  do not coincide. For  $\bar{\theta}$ , the effective stiffness of the chain with even-numbered nodes is positive and monotonically decreases with the increase of the number of nodes; for  $-\bar{\theta}$ , it presents a negative stiffness and the magnitude of the stiffness also decreases with the increase of the number of nodes.

The effective stiffnesses of the chain with odd-numbered nodes are shown in Fig. 4(e). The red and black triangles correspond to the results for  $\bar{\theta}$  and  $-\bar{\theta}$  respectively. The effective stiffness still presents a monotonically decreasing rule with the increase of the number of nodes, however surprisingly, it is completely different from that of the chain with even-numbered nodes, namely the effective stiffnesses under  $\bar{\theta}$  and  $-\bar{\theta}$  completely coincide, as shown in Fig. 4(e).

In order to explain the different characteristics of the effective stiffness of the

chains with odd and even-numbered nodes, the attenuation lengths of the finite boundary states of the chains are calculated (See Supplement A for details), shown in Figs. 4(c) and (f), respectively. Fig. 4(c) show that for  $\bar{\theta}$  and  $-\bar{\theta}$ , the attenuation lengths of the chains with even-numbered nodes converge well to the characteristic attenuation length of the periodic structure with the increase of the node number. The above results show that the characteristic attenuation length of the chain before and after the equilibrium-angle inversion does not change, namely, the non-coincidence of the effective stiffness of the chain with even-numbered nodes before and after the equilibrium-angle inversion does not come from the change of the characteristic attenuation length.

$$0 = -k_{\theta}(\delta\theta_{n+1} + \delta\theta_{n-1} + 4\delta\theta_n) + k_s(\delta\theta_{n+1} + \delta\theta_{n-1} - 2\delta\theta_n)l^2 \cos\bar{\theta} - 2k_t l^2 \sin^2\bar{\theta}, \quad (18)$$

In addition, it can be seen from the governing equation Eq.(18) that when  $\bar{\theta} \rightarrow -\bar{\theta}$ , the governing equation remains unchanged, which indicates that the inversion of the equilibrium angle does not affect the response of the periodic structure, and therefore does not cause the change of the characteristic attenuation length  $\lambda^*$ . On the other hand, Fig. 4(f) shows the attenuation lengths of the boundary state of the one-sided excited chain with odd-numbered nodes for  $\bar{\theta}$  and  $-\bar{\theta}$ . The results show that the attenuation lengths of finite structures with odd-numbered nodes under  $\bar{\theta}$  and  $-\bar{\theta}$  not only converge to the characteristic attenuation length with the increase of the number of nodes, but also completely coincide at each node. This phenomenon reflects that its underlying mechanism has a special symmetry, namely there is a mirror symmetry relationship between the chains with initial equilibrium angles  $\bar{\theta}$  and  $-\bar{\theta}$ . Thus, the displacement  $u_n^-$  and rotation-angle distributions  $\delta\theta_n^-$  of the chain for  $-\bar{\theta}$  can be

obtained by variable substitution, namely  $u_n^- = -u_{M-n}^+$ ,  $\delta\theta_n^- = -\delta\theta_{M-n}^+$ .

However, the chain with even-numbered nodes does not have the mirror symmetry mentioned above, and it is only a kind of structure symmetric with respect to the central axis. For example, for  $\bar{\theta}$ , the displacement and rotation-angle distributions only satisfy  $u_n^+ = -u_{M-n}^+$  and  $\delta\theta_n^+ = \delta\theta_{M-n}^+$ . The different symmetries of the underlying mechanism of the chains with odd and even nodes directly lead to the abnormal size effect behaviors, namely before and after the equilibrium-angle inversion, the stiffnesses of the chain with odd nodes are coincident but those of the chain with even nodes are not coincident. The attenuation length of the finite structure can well represent the symmetry of the underlying mechanism, namely, if the attenuation lengths of each node for  $\bar{\theta}$  and  $-\bar{\theta}$  are completely coincident, there is a mirror-symmetry relationship between the two steady states. In the analysis of multi-stable structures, compared with the characteristic attenuation length  $\lambda^*$ , which can only characterize the properties of large-sized structures (periodic structures), the attenuation length  $\lambda$  of finite structures can more accurately characterize the properties of structures. Namely, by using the attenuation length  $\lambda$ , the symmetry between chain steady-states can also be characterized in small-sized structures (finite structures). When the structures tend to be large-sized,  $\lambda$  gradually converge to  $\lambda^*$ , the deformation of the chain gradually changes to a mechanism of large size (soft mode) (see Supplement B for details) .

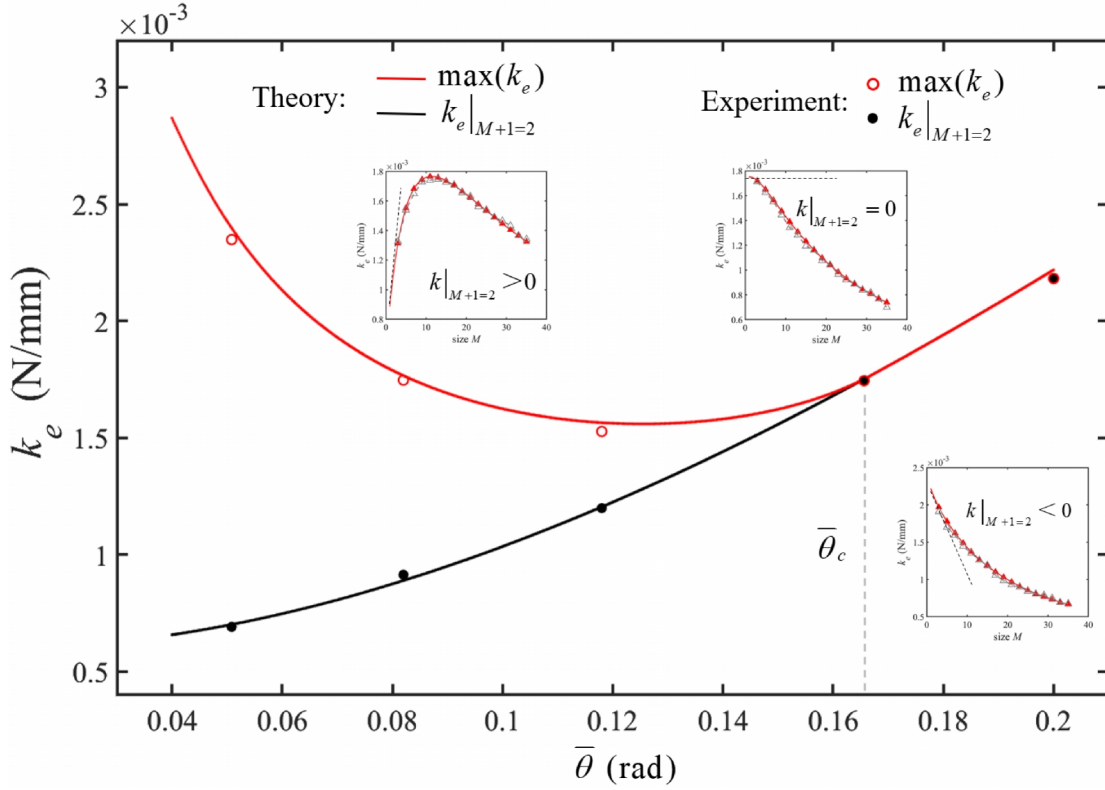


Fig. 5. The maximum effective stiffness  $\max(k_e)$  of the bistable chain vs. initial equilibrium angle  $\bar{\theta}$ , shown by the red solid line. The black line in the figure represents the relationship between the effective stiffness  $k_e|_{M+1=2}$  of the 2-node structure and the initial equilibrium angle  $\bar{\theta}$ , which intersects with the red line at  $\bar{\theta} = \bar{\theta}_c$ . The three illustrations on the top left, top right and bottom right are respectively the size effects corresponding to  $\bar{\theta} < \bar{\theta}_c$ ,  $\bar{\theta} = \bar{\theta}_c$  and  $\bar{\theta} > \bar{\theta}_c$ , where  $k|_{M=1}$  is the slope of the effective stiffness at  $M=1$ .

It can be seen from Figs. 4(b) that for a large value of  $\bar{\theta}$ , the stiffness of one-dimensional chain with even-numbered nodes varies monotonically with the number of node, which is inconsistent with the non-monotonic variation of the size effect of one-dimensional monostable counter-rotation metamaterial chains with even-numbered nodes (the effective stiffness has a maximum value) [21]. In order to clarify conditions for emerging of non-monotonic size effects of the bistable chain, the relationship between the abnormal non-monotonic size effect and  $\bar{\theta}$  is analyzed. Firstly, the maximum values of effective stiffnesses of the bistable chain for different

number of nodes are calculated, the results are shown by the red solid line in Fig. 5. It is shown that the maximum effective stiffness varies with  $\bar{\theta}$  non-monotonically, there is a minimum value, and the maximum effective stiffness  $\max(k_e)$  intersects with the effective stiffness  $k_e|_{M+1=2}$  of the 2-node structure at  $\bar{\theta} = \bar{\theta}_c$ . This phenomenon indicates that the size effect is non-monotonic when  $\bar{\theta} < \bar{\theta}_c$ , which is also verified in the illustration on the top left ( $k|_{M=1} > 0$ ),  $k|_{M=1}$  is the slope of the effective stiffness at  $M=1$ ). Illustrations on top right and bottom right are respectively the size effects corresponding to  $\bar{\theta} = \bar{\theta}_c$  and  $\bar{\theta} > \bar{\theta}_c$ , respectively. When  $\bar{\theta} = \bar{\theta}_c$ , the size effect is at the critical point between monotonic and non-monotonic conditions ( $k|_{M=1} = 0$ ). When  $\bar{\theta} > \bar{\theta}_c$ , the non-monotonic size effect disappears, and the size effect changes to be monotonic ( $k|_{M=1} < 0$ ).

#### 4. Bifurcation behaviors of size effects

In order to investigate the overall lateral stiffness of a one-dimensional chain, a nominal stiffness is defined as

$$k_n = \frac{F}{\Delta L_n}, \quad (19)$$

where  $\Delta L_n$  is the distance change of centers of crosses at both ends of the chain (see Supplement B for details). The nominal stiffness eliminates the influences of the rotation-angles at the two ends, and presents the overall lateral stiffness of the chain more intuitively. Figs. 6 (a), (b) are the nominal stiffness and effective stiffness vs. number of nodes  $M$  of the chain with even-numbered nodes, respectively. It is shown in Fig. 6 (a) that the size effect has a bifurcation behavior at the critical point  $\bar{\theta} = \bar{\theta}^*$ . Firstly, when  $\bar{\theta} < |\bar{\theta}^*|$ , it appears a normal size effect, namely, with the increase of the number of nodes, the size of the absolute value of the stiffness gradually decays to



zero after experiencing an extreme value; when  $\bar{\theta} = \bar{\theta}^*$ , the stiffness does not change with the increase of  $M$  after a certain number of nodes, namely there is no size effect. When  $\bar{\theta} > |\bar{\theta}^*|$ , after experiencing an extreme value, the stiffness presents an abnormal size effect, namely, the absolute value of stiffness increases with the increase of  $M$ . In addition, the effective stiffnesses of the one-dimensional chain are calculated, the results are shown in Fig. 6(b). It is shown that the effective stiffness also has a bifurcation behavior at the critical point  $\bar{\theta} = \bar{\theta}^*$ , and the bifurcation lines of the effective stiffness are proportional to those of the nominal stiffness.

Theoretical analysis in Supplement material B shows that the reason for the occurrence of the disappearance of the size effect when  $\bar{\theta} = \bar{\theta}^*$  is as follows: when  $\bar{\theta} = \bar{\theta}^*$ , the coefficient matrix  $A(\bar{\theta})$  of the force and displacement is rank-deficient, namely, even if the number of nodes changes, the ratio of the displacement and the force remains unchanged, so the stiffness remains unchanged when the value of  $M$  increases, namely, no dimensional effect occurs (see Supplement B for details). For the chain with even-numbered nodes, the nominal stiffness is  $k_g = F / (u_0 - u_M)$ , the effective stiffness is  $k_e = F / [u_0 - u_M + l(\delta\theta_0 \pm \delta\theta_M)]$ . Previous studies have found that the ratio (polarization index) of displacement and rotation-angle in each node of a bistable chain that meets periodic boundary conditions remains the same [24]. When the stiffness expression is simplified by using the polarization index, the equivalent stiffness in a sufficiently long chain can be approximately simplified as  $k_e = k_g / (1 + 1/\gamma)$ , namely there is a proportional relationship between the effective stiffness and the nominal stiffness. Therefore, the effective stiffness and the nominal stiffness produce bifurcation behaviors at the same value of  $\bar{\theta}^*$ .

The above phenomenon indicates that the nominal stiffness, which is easier to

test compared to the effective stiffness, can also be used to characterize the stiffness of bistable chains. On the other hand, this phenomenon corresponds to the property that the polarization index of each node is the same, which is a unique property of periodic structures (large-sized bistable chains), thus this phenomenon reflects that the mechanism of the periodic structure (soft mode) dominates the deformation of the chain when  $M$  is large enough. When  $M \gg 1$ , the distribution patterns of displacement ( $u_n^{\text{L or R}}$ ) and rotation angle ( $\delta\theta_n^{\text{L or R}}$ ) at both ends are almost consistent with the soft mode (see Supplement B for details).

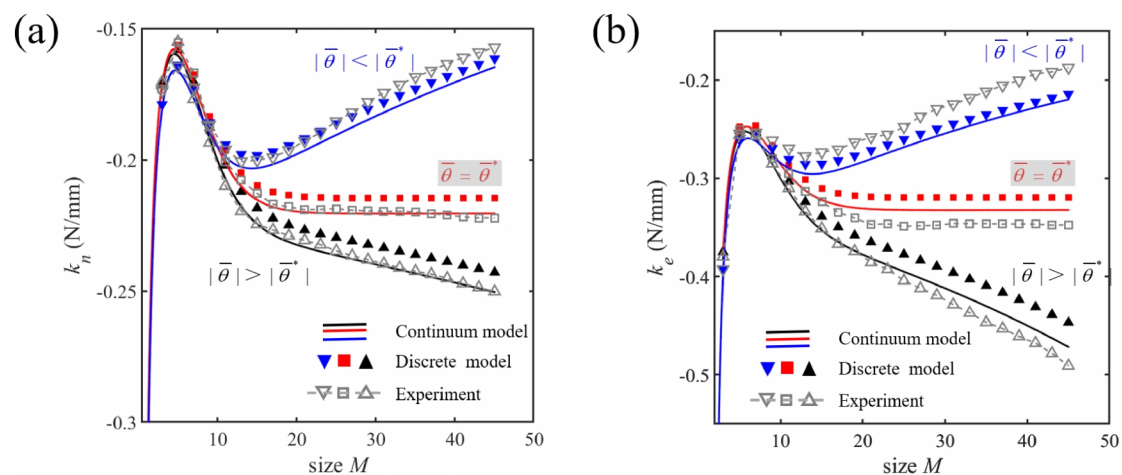


Fig. 6. Bifurcation behaviors of size effects. (a), (b) are bifurcations of nominal stiffness and equivalent stiffness of the chain with even-numbered nodes, respectively, and both have the same critical point  $\bar{\theta} = \bar{\theta}^*$ .

## 5. Conclusions

In this work, the effective stiffness of bistable counter-rotating metamaterial chains is investigated, and abnormal size effects are found. The two steady states exhibit completely different size effects for the chains with even-numbered nodes, while they exhibit same size effects for the chains with odd-numbered nodes, and it is found that this abnormal behavior can be characterized by the attenuation length of

the finite structure. Furthermore, conditions for emerging of abnormal non-monotonic size effect are clarified. In addition, for the influence of the initial equilibrium angle on the size effect, an abnormal bifurcation behavior of size effects is found in the chain with even-numbered nodes, the closed solution is derived to calculate the bifurcation point and reveal the mechanism of this phenomenon. The above findings provide a new underlying mechanism for the design of adaptive intelligent structures with complex rules in robots, which has important theoretical and application values.

### Supplement A: Attenuation length of finite structures

In Part 2, it is showed that the boundary state in the periodic structure has a attenuation factor  $q=e^{-1/\lambda^*}$ . The relationship between the characteristic attenuation length  $\lambda^*$  and the attenuation factor  $q$  is:

$$\lambda^* = -\frac{1}{\ln q} . \quad (\text{B.1})$$

(1) The attenuation length of the chain with even-numbered nodes

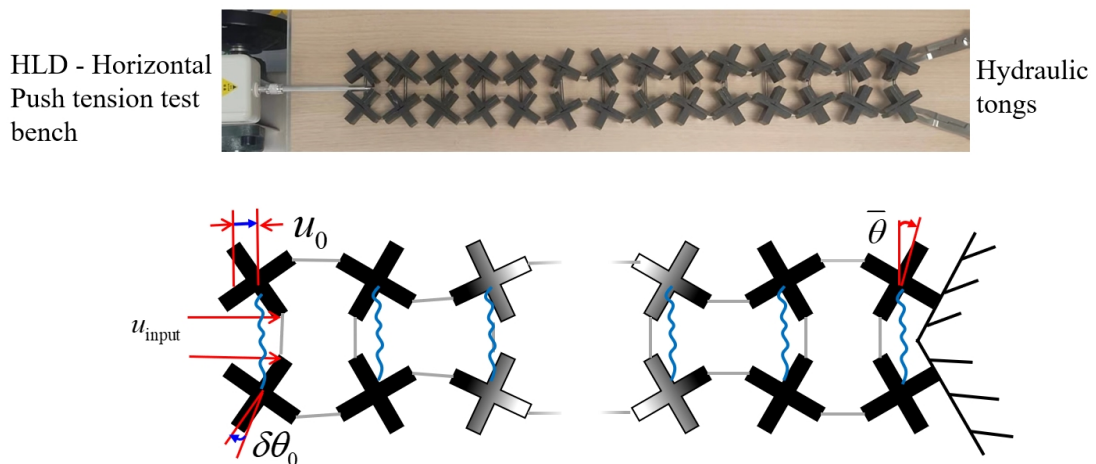


Fig. A.1. Experimental photo of the chain with even-numbered nodes (top), diagram of the left boundary state of the chain (bottom).

For the chain with even-numbered nodes, the right end is constrained by the

fixed constraint ( $\delta\theta_M = u_M = 0$ ), and the force of  $F/2$  is applied at the joints between the shim and the crosses at the left end, and the chain finally forms a left boundary state, as shown in Fig. A.1. The attenuation factor between the nodes of the finite structure is  $q_n = \delta\theta_n / \delta\theta_{n-1}$ , the attenuation length of the finite structure can be calculated as follows:

$$\lambda = -\frac{\sum_{n=1}^M 1/\ln q_n}{M-1}. \quad (\text{A.2})$$

(2) Attenuation length of the chain with odd-numbered nodes

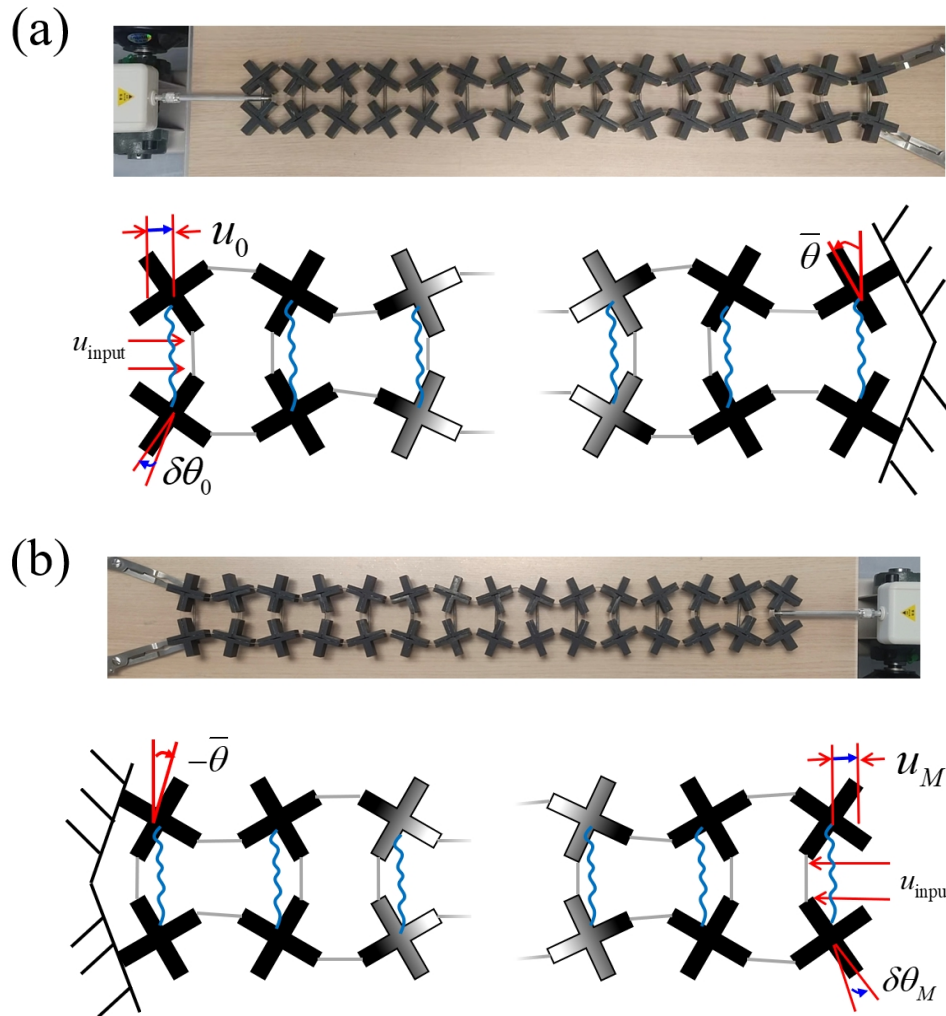


Fig. A.2. (a) The photo of the chain with odd-numbered nodes with initial equilibrium angle  $\bar{\theta}$  (top), and the schematic diagram of the left boundary state of the chain with odd-numbered nodes with initial equilibrium angle  $\bar{\theta}$  (bottom). (b) The photo of the chain with odd-numbered nodes with initial

equilibrium angle  $-\bar{\theta}$  (top), and the schematic diagram of the left boundary state of the chain with odd-numbered nodes with initial equilibrium angle  $-\bar{\theta}$  (bottom).

For the chain with odd-numbered nodes with initial equilibrium angle  $\bar{\theta}$ , the right end of the chain is constrained by the fixed constraint, and the left end of the chain is excited, and the chain finally forms a left boundary state, as shown in Fig. A2 (a). For the chain with initial equilibrium angle  $-\bar{\theta}$ , the left end of the chain is constrained by the fixed constraint, and the right end of the chain is excited, and the chain eventually forms a right boundary state, as shown in Fig. A2 (b). The attenuation lengths of two boundary states in a finite structure can be calculated by Eq. (A. 2).

### Supplement B: Modeling of the chain with even-numbered nodes without size effects

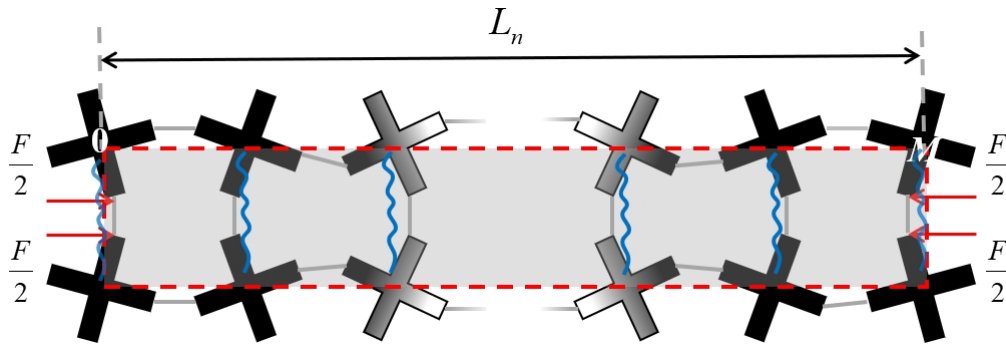


Fig. B1. Diagram of the nominal stiffness

The expression for defined nominal stiffness is as follows:

$$k_n = \frac{F}{\Delta L_n} = \frac{F}{u_0 - u_M} . \quad (\text{B.1})$$

The schematic diagram is shown in Fig. B1. Substituting Eq.(A.11) into Eq.(B.1) yields:

$$k_n = \frac{F}{-4\sin\bar{\theta}C_1n^*(1-e^{M/n^*})-2D_1M}, \quad (\text{B.2})$$

For a large value of  $M$ , the dominant term of the denominator of nominal stiffness  $k_n$  is  $4\sin\bar{\theta}C_1n^*e^{M/n^*}$ . In order to obtain no size effect when  $\bar{\theta} = \bar{\theta}^*$ , it is required that when the number of nodes changes, the proportion of the displacement  $4\sin\bar{\theta}C_1n^*e^{M/n^*}$  generated by the force and the size of the force  $F$  remains unchanged, namely, when the number of nodes  $M$  changes, the ratio of  $F$  and  $C_1e^{M/n^*}$  remains unchanged.

For a large value of  $M$ , boundary conditions Eqs. (1-a) and (2-c) of the chain with even-numbered nodes are simplified to

$$\begin{bmatrix} f_1(\bar{\theta}) & -1 \\ f_2(\bar{\theta}) & -1 \end{bmatrix} \begin{bmatrix} C_1e^{M/n^*} \\ F \end{bmatrix} = 0, \quad (\text{B.3})$$

where  $f_1(\bar{\theta}) = [-k_\theta(\frac{1}{e^{1/\lambda^*}} + 3) - k_t l^2 \sin^2 \bar{\theta}(\frac{1}{e^{1/\lambda^*}} + 1) + k_s l^2 \cos \bar{\theta}(\frac{1}{e^{1/\lambda^*}} - 1) - 2k_t l^2 \sin^2 \bar{\theta} +$

$2k_t l^2 \sin^2 \bar{\theta} n^* (-\frac{1}{e^{1/\lambda^*}} + 1)] / (l \cos \bar{\theta})$ ,  $f_2(\bar{\theta}) = 2k_t l \sin \bar{\theta} [\lambda^* (-\frac{1}{e^{1/\lambda^*}} + 1) + \frac{1}{e^{1/\lambda^*}} + 1]$ . A matrix of

coefficients is defined, namely  $A(\bar{\theta}) = \begin{bmatrix} f_1(\bar{\theta}) & -1 \\ f_2(\bar{\theta}) & -1 \end{bmatrix}$ . Eq.(B.3) has a non-trivial solution

when the coefficient matrix is rank-deficient, and the ratio of  $F$  to  $C_1e^{M/n^*}$  remains unchanged when  $M$  changes. The calculation formula of  $\bar{\theta}^*$  is as follows:

$$\det A(\bar{\theta}) \Big|_{\bar{\theta}=\bar{\theta}^*} = 0, \quad (\text{B.4})$$

where,  $A(\bar{\theta})$  is the coefficient matrix of Eq. (B.3), we can obtain  $\bar{\theta}^* = -0.70051$ .

While in Fig. 6, the results of  $\bar{\theta}^*$  from discrete and continuous models are almost identical, which proves the feasibility of calculating bifurcation points by using Eq.(B.4).

According to Eqs. (10) and (11), for a large value of  $M$ , the approximate form of the displacement and rotation-angle solutions at the left and right ends is as follows:

$$\begin{bmatrix} \delta\theta_n^L \\ u_n^L \end{bmatrix} = \begin{bmatrix} C_1 \\ 2l \sin \bar{\theta} \lambda^* C_1 \end{bmatrix} e^{(M-n)/\lambda^*}, \text{ for } n \rightarrow 0 \quad (\text{B.5-a})$$

$$\begin{bmatrix} \delta\theta_n^R \\ u_n^R \end{bmatrix} = \begin{bmatrix} C_1 \\ -2l \sin \bar{\theta} \lambda^* C_1 \end{bmatrix} e^{n/\lambda^*}, \text{ for } n \rightarrow M \quad (\text{B.5-b})$$

Under the periodic boundary conditions of the bistable chain (soft mode), the solution form of the displacement and rotation-angle is as follows:

$$\begin{bmatrix} \delta\theta_n \\ u_n \end{bmatrix} = \begin{bmatrix} \pm \tilde{\delta}\theta \\ \pm 2l \sin \bar{\theta} \lambda^* \tilde{\delta}\theta \end{bmatrix} e^{n/\lambda^*}, \quad (\text{B.6})$$

where  $\tilde{\delta}\theta$  is an integral constant, the value of  $\tilde{\delta}\theta$  and the sign ( $\pm$ ) in the equation depend on the initial excitation type, namely the “+” sign is taken when there is left boundary state and the “-” sign is taken when there is a right boundary state. By combining Eqs. (B.5) and (B.6), it can be obtained that the displacement and rotation-angle distributions for the excitation at both ends are almost consistent with those of the soft mode when the value of  $M$  is large.

## References

- [1] K. Bertoldi, V. Vitelli, J. Christensen, M. van Hecke, Flexible mechanical metamaterials, *Nature Reviews Materials* 2(11) (2017) 17066.
- [2] B. M. Goldsberry, M. R. Haberman, Negative stiffness honeycombs as tunable elastic metamaterials, *J. Appl. Phys.* 123(9) (2018) 091711.
- [3] H. Yasuda, J. Yang, Reentrant Origami-Based Metamaterials with Negative Poisson's Ratio and Bistability, *Phys. Rev. Lett.* 114(18) (2015) 185502.
- [4] D. Misseroni, P. P. Pratapa, K. Liu, G. H. Paulino, Experimental realization of

tunable Poisson's ratio in deployable origami metamaterials, *Extreme Mechanics Letters* 53 (2022) 101685.

[5] J. Bauer, L. R. Meza, T. A. Schaedler, R. Schwaiger, X. Zheng, L. Valdevit, Nanolattices: an emerging class of mechanical metamaterials, *Advanced Materials* 29(40) (2017) 1701850.

[6] H. Yang, W. H. Müller, Size effects of mechanical metamaterials: a computational study based on a second-order asymptotic homogenization method, *Archive of Applied Mechanics* 91(3) (2021) 1037-1053.

[7] J. Frame, M. Wheel, P. Riches, A numerical investigation and experimental verification of size effects in loaded bovine cortical bone, *International Journal for Numerical Methods in Biomedical Engineering* 34(1) (2018) e2903.

[8] R. D. Mindlin, Second gradient of strain and surface-tension in linear elasticity, *International Journal of Solids and Structures* 1(4) (1965) 417-438.

[9] D. Ieşan, On the linear theory of micropolar elasticity, *International Journal of Engineering Science* 7(12) (1969) 1213-1220.

[10] A. J. Beveridge, M. A. Wheel, D. H. Nash, The micropolar elastic behaviour of model macroscopically heterogeneous materials, *International Journal of Solids and Structures* 50(1) (2013) 246-255.

[11] A. Waseem, A. J. Beveridge, M. A. Wheel, D. H. Nash, The influence of void size on the micropolar constitutive properties of model heterogeneous materials, *European Journal of Mechanics - A/Solids* 40 (2013) 148-157.

[12] M. McGregor, M. A. Wheel, On the coupling number and characteristic length of micropolar media of differing topology, *Proceedings of the Royal Society A: Mathematical, Physical and Engineering Sciences* 470(2169) (2014) 20140150.

[13] J. F. C. Yang, R. S. Lakes, Experimental study of micropolar and couple stress



- elasticity in compact bone in bending, *Journal of Biomechanics* 15(2) (1982) 91-98.
- [14] K. Choi, J. L. Kuhn, M. J. Ciarelli, S. A. Goldstein, The elastic moduli of human subchondral, trabecular, and cortical bone tissue and the size-dependency of cortical bone modulus, *Journal of Biomechanics* 23(11) (1990) 1103-1113.
- [15] M. A. Wheel, J. C. Frame, P. E. Riches, Is smaller always stiffer? On size effects in supposedly generalised continua, *International Journal of Solids and Structures* 67-68 (2015) 84-92.
- [16] B. Deng, A. Zareei, X. Ding, J. C. Weaver, C. H. Rycroft, K. Bertoldi, Inverse design of mechanical metamaterials with target nonlinear response via a neural accelerated evolution strategy, *Advanced Materials* 34(41) (2022) 2206238.
- [17] C. Coulais, D. Sounas, A. Alu, Static non-reciprocity in mechanical metamaterials, *Nature* 542(7642) (2017) 461-464.
- [18] B. Deng, J. Raney, V. Tournat, K. Bertoldi, Elastic vector solitons in soft architected materials, *Physical review letters* 118(20) (2017) 204102.
- [19] B. Deng, P. Wang, Q. He, V. Tournat, K. Bertoldi, Metamaterials with amplitude gaps for elastic solitons, *Nature communications* 9(1) (2018) 3410.
- [20] B. Deng, V. Tournat, P. Wang, K. Bertoldi, Anomalous collisions of elastic vector solitons in mechanical metamaterials, *Physical review letters* 122(4) (2019) 044101.
- [21] C. Coulais, C. Kettenis, M. van Hecke, A characteristic length scale causes anomalous size effects and boundary programmability in mechanical metamaterials, *Nature Physics* 14(1) (2018) 40-44.
- [22] B. Deng, M. Zanaty, A.E. Forte, K. Bertoldi, Topological solitons make metamaterials crawl, *Physical Review Applied* 17(1) (2022) 014004.
- [23] H. Yasuda, L. Korpas, J. Raney, Transition waves and formation of domain walls in multistable mechanical metamaterials, *Physical Review Applied* 13(5) (2020)

054067.

[24] Z. H. Tang, T. F. Ma, S. H. Z. Li, H. Chen, B. Y. Su, P. F. Kang, J. Wang, P. Li, B. W. Wu, Z. H. Qian, H. Shi, Polarization-dependent boundary modes in nonlinear mechanical metamaterials, *International Journal of Mechanical Sciences* 258 (2023) 108584.